Feasible Coefficient Region Analysis and Dual-Loop Adaptive Feedback Control for Transient Stability of VSG Under Severe Grid Voltage Sag

Kun Sun, Wei Yao, *Senior Member, IEEE*, Qihang Zong, Jinyu Wen, *Member, IEEE*, and Lin Jiang, *Member, IEEE*

Abstract—**Aiming at the transient instability and overcurrent issues of the virtual synchronous generator (VSG) under severe grid voltage sag, the accurate and simultaneous control for the phase angle and current of VSG is hard to be achieved without using the fault information. And the requirement of the grid code for the reactive current should be also considered. To address the issues, this paper proposes a non-fault information based dual-loop adaptive feedback control to take transient angle stability, current limitation and the demand of the reactive current of VSG into account. First the large-signal model of VSG with a dual-loop control is built. To design the feedback coefficients, the feasible coefficient region under different fault degrees and cases is analyzed subsequently. It provides reference for the curve fitting, which is further applied in the self-adaptive regulation of the feedback coefficients. Thereby, a dual-loop adaptive feedback control is realized based on an additional reactive power feedback loop. With the proposed control scheme, all of the three control objectives can be achieved without the fault information, since the feedback coefficients are within the feasible coefficient region by the self-adaptive regulation. Finally, the effectiveness and robustness of the proposed control scheme for both VSG and a paralleled system of VSG and grid-following (GFL) converter are validated by the simulation results and the experimental results.**

Index Terms—**virtual synchronous generator, transient angle stability, current limitation, reactive current, feasible coefficient region, adaptive feedback control**

I. Introduction

Renewable energy resources (RES) are normally integrated to the power grid by the voltage source converter (VSC), which is controlled by the grid-following (GFL) or grid-forming (GFM) method for the different control objectives [1]. The GFL converter is normally connected to a strong power grid and aims to generate power by maximum power point tracking scheme. To overcome the lack of inertia support of the GFL converter, the virtual synchronous generator (VSG), a typical GFM converter, is developed. VSG is able to emulate the

voltage and frequency independently [2]. However, VSG is more susceptible to the physical damage with low overcurrent characteristics of the synchronous generator and establishes capabilities compared with the GFL converter [3]. It also suffers from the transient angle instability during fault such as a grid voltage sag [4]. Therefore, both the transient angle stability and current limitation of VSG attract a lot of attention currently [5]. In addition, the requirement of the grid code for VSG under severe grid voltage sag should be also considered.

The transient angle stability of VSG describes the ability to synchronize with the grid under large disturbance, which can be enhanced generally by two categories of methods [6]-[13]. One method is to change the power reference of VSG, and reducing the reference of active power control loop (APCL) is a straightforward way by solving the active power imbalance. The grid voltage sag is detected and feeds back to APCL to regulate the active power reference in [6], [7]. Compared with [8], by feedforwarding the angular frequency difference from APCL, the active power reference can be regulated without fault detection though an additional high-pass filter is required. In [9], increasing the reference of reactive power control loop (RPCL) is beneficial to the transient angle stability. Thus, the angular frequency difference from APCL can also be introduced into RPCL to regulate the reactive power reference [10]. The other method is to modify the control loops or coefficients to improve the transient angle stability of VSG. The damping and inertia coefficient is regulated in [11]. But the reasonable determination of the coefficients is hard. In [12], a mode-switching adaptive method is proposed, which could achieve ride-through without an equilibrium point due to a switched control coefficient in APCL for the active power reference regulation. Similarly, a switched control coefficient is applied in RPCL for the reactive power reference regulation [13]. However, the mode-switching block is complicated.

The current limitation is another important issue of VSG to avoid the physical damage, which can be realized generally by two categories of methods [14]-[21]. One method is to limit the current reference directly with a saturation block, and then the converter works as a current source during fault. But the transient angle stability with the saturation block is deteriorated [14], [15]. To maintain the synchronization during fault, the GFM control can switches to the GFL control with a backup phase-lock loop (PLL) [16]. However, there is a problem to switch back to the GFM control after fault. Even worse, the characteristics of the GFM control are lost during fault. To

TABLE I
COMPARISON OF THE TRANSIENT ANGLE STABILITY ENHANCED METHODS

Methods	Control objectives			No need for fault information
	Transient angle stability	Current limitation	The grid code for the reactive current	
Reduce P reference in APCL [6-8]	√	×	×	×
Improve Q reference in RPCL [9-10]	√	×	×	×
Change inertia and damping in APCL [11]	√	×	×	×
Optimal calculation of the saturated current angle or virtual impedance [15], [21]	√	√	×	×
Adaptive mode-switching control in APCL [20]	√	√	×	√
Dual-loop adaptive mode-switching control [25]	√	√	√	×
Dual-loop parameter-switching control [27]	√	√	√	×
Dual-loop adaptive feedback control (proposed in this paper)	√	√	√	√

avoid the issue, the other method of voltage limitation is applied. For instance, a virtual impedance (VI) is applied to limit the current by reducing the voltage reference [17]. It can also be realized by a virtual admittance to limit the current fast with the current loop [18]. Nevertheless, the application of VI is usually harmful to the transient angle stability, which limits its practicability [19]. To avoid the negative influence, a transient virtual resistor is activated during fault and then deactivated [20]. In [21], a *dq* frame asymmetrical VI with the ingenious set is proposed to avoid the negative transient influence. However, the reasonable design of the virtual resistor or VI is hard.

In addition, the requirement of the grid code for VSG during fault should be considered as well. For the continuous power generation, RESs are required to remain connected with the grid to realize low voltage ride-through and to inject reactive current to support the grid [22]. The reactive current of RESs during normal state is usually set to zero, while it is determined by the grid code during low voltage ride-through (LVRT). In special, RESs are supposed to inject pure reactive current under a severe grid voltage sag which is lower than 50%, and active current is set to zero for the current limitation [23], [24]. For the safe and stable operation of VSG, how to comply with the grid code for the reactive current injection under prerequisite of the transient stability and current limitation is worthy of study.

However, the transient angle stability, current limitation and the demand of the grid code of VSG have not been considered simultaneously in the most references. There is a conflict among the three control objectives. For instance, the transient angle stability enhancement may provoke the current limitation [9], [10]. In contrast, the current limiter or VI may drivers the converter into transient instability [14], [15]. To address this issue, the phase angle and current can be both precisely controlled by a two-stage simultaneous control scheme based on the fault information [25]. A dual-loop feedback control is then proposed to achieve the transient angle stability and current limitation without using the fault information [26]. But how to select the reasonable coefficients is missing. In [27], the comprehensive transient stability enhancement control strategy of VSG considering power angle stability and current limitation is realized with the dual-loop parameter-switching control of the voltage difference. In addition, the requirement of the grid code for VSG is also contradictory to the current limitation during fault. The converter is required to inject expected reactive current to support the grid during fault while the increased reactive power reference is beneficial to the transient angle stability. However, to increase the reactive current goes against the requirement of the current limitation.

Overall, the above methods have disadvantages individually, and there are three main problems need to be solved. First, the methods based on the fault information acquisition such as the parameter or mode-switching control is not effective when the fault detecting device is not available. The fault detecting device may not be installed on all of the lines for the practical project due to the cost, while its accuracy and speed are also limited by the fault detecting method and the necessary equipment. Second, the design of the feedback coefficients is missing, which should be within the feasible coefficient region. Last but not least, the requirement of the grid code for the reactive current of VSG during fault is not considered, especially under a severe grid voltage sag. It is hard to achieve the demand of the reactive current while the total current does not provoke the limit. To clearly describe the pros and cons of the above methods, a comparison table is given in Table I.

To overcome the disadvantages of the references, this paper proposes a non-fault information based dual-loop adaptive feedback control to take transient angle stability, current limitation and the demand of the grid code of VSG into account. Based on the large-signal model of VSG with a dual-loop feedback control, the feasible coefficient region under different cases and fault degrees is analyzed and provides reference for the curve fitting, which is further applied in the self-adaptive regulation of the feedback coefficients. Thereafter, a dual-loop adaptive feedback control is realized based on an additional reactive power feedback loop without using the fault information. With the proposed control scheme, all of the three control objectives can be achieved since the feedback coefficients are within the feasible coefficient region due to the self-adaptive regulation.

The main contributions of this paper are listed as follows:
- A non-fault information based dual-loop adaptive feedback control is proposed, which can simultaneously achieve three control objectives of transient angle stability, current limitation and requirement of the grid code for the reactive current of VSG, with robustness to the parameter errors.
- The proposed control scheme is fulfilled by the feasible coefficient region analysis and the dual-loop adaptive feedback control based on an additional reactive power feedback loop. Besides, the control scheme can be applied in both VSG and a paralleled system of VSG and VSC.
- The feasible coefficient region analysis for the feedback coefficients of the dual-loop feedback control of VSG under different cases is carried out. The three control objectives can be realized when the reasonable sets of

feedback coefficients are derived and applied in APCL and RPCL of VSG, with robustness to the parameter errors.

- An additional reactive power feedback loop is proposed to realize the dual-loop adaptive feedback control. By the curve fitting of the feasible coefficient region, the reasonable feedback coefficients are derived through the self-adaptive regulation without using the fault information.

The remainder of this paper is organized as follows. In Section II, the large-signal models of VSG and the paralleled system with a dual-loop feedback control of VSG are built. In Section III, the feasible coefficient region of the feedback coefficients under different fault degrees and cases are analyzed. With the curve fitting due to the analysis, a dual-loop adaptive feedback control is proposed in Section IV. The effectiveness and robustness of the proposed control scheme are validated by simulation in Section V. The effectiveness of the proposed control scheme is also validated by experiment in Section VI. Conclusions are drawn in Section VII.

II. A Dual-Loop Feedback Control of VSG

In this Section, the large-signal models of VSG and the paralleled system of VSG and VSC are built respectively with a dual-loop feedback control.

A. System Configuration

The system structure of a VSG connected to the grid is depicted in Fig. 1. The internal voltage of VSG is expressed as $E \angle \theta_{vsg}$ while the grid voltage is $U_g \angle \theta_g$. Taking the grid voltage as a reference, the power angle δ is equal to the phase difference between U_g and E, which is $\delta=\theta_{vsg}-\theta_g$. Z_{line} represents for the impedance of the parallel-circuit transmission line. Z_T is the transformer's leakage impedance. C_f, L_f are the capacitor and inductance of the filter. ω_n is the rated angular frequency.
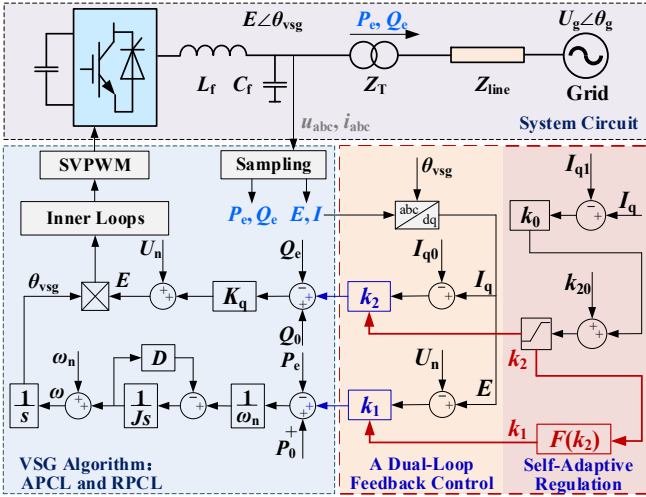

Fig. 1. System structure and the dual-loop feedback control of VSG.

As shown in Fig. 1, the phase and the internal voltage amplitude commands of VSG, θ_{vsg} and E, are produced by APCL and RPCL respectively. Note that the inner voltage and current loops can be considered as a unity gain when the reference is tracked ideally during the transient process, due to the decoupled timescales between the outer and inner loops [9]. Therefore, the transient angle stability of VSG is mainly determined by APCL and RPCL. Similarly, the dynamic influence of the capacitor and inductor can also be ignored.

B. Modelling of VSG with a Dual-Loop Feedback Control

The swing equation of APCL can be modelled as

$$J\ddot{\delta} = -D\dot{\delta} + (P_0 - P_e) \tag{1}$$

where, J is the virtual inertia, D is the damping coefficient, P_e and P_0 are the active power and its reference of VSG.

In addition, the droop control of RPCL is modelled as

$$E = K_q(Q_0 - Q_e) + U_n \tag{2}$$

where, U_n is the nominal voltage, K_q is the droop coefficient. Q_e and Q_0 are the reactive power and its reference of VSG.

Normally, the total system impedance can be expressed as $Z=Z_{line}+Z_T=R+jX$. And then the output active power and reactive power of VSG can be expressed as

$$\begin{cases} P_e = -\alpha U_g E \cos\delta + \beta U_g E \sin\delta + \alpha E^2 \\ Q_e = -\alpha U_g E \sin\delta - \beta U_g E \cos\delta + \beta E^2 \end{cases} \tag{3}$$

where, $\alpha=R/(R^2+X^2)$, $\beta=X/(R^2+X^2)$.

According to (3), the steady-state output current of VSG in dq frame can be derived as

$$\begin{cases} I_d = \dfrac{-RU_g\cos\delta + XU_g\sin\delta + RE}{R^2+X^2} \\ I_q = \dfrac{-RU_g\sin\delta - XU_g\cos\delta + XE}{R^2+X^2} \end{cases} \tag{4}$$

By substituting (3) into (2), the relationship between E and δ can be revealed as (5).

By substituting (5) into (3), the relationship between P_e and δ can be revealed. Thus, the P_e-δ curve with different U_g, K_q can be plotted. By combining (1) and (3), the second order nonlinear differential equation of VSG can be derived as

$$J\ddot{\delta} = -D\dot{\delta} + [P_0 - (-\alpha U_g E \cos\delta + \beta U_g E \sin\delta + \alpha E^2)] \tag{6}$$

Thereafter, the transient performance of VSG during fault can be analyzed due to (6).

According to the IEEE standard 1159-2019 [28], the typical range of grid voltage sags is between 0.1 and 0.9 pu. And the IEEE standard 1547-2018 [29] requires that the converters needs to remain connected with the grid about 1 s even if the grid voltage falls a little below 0.5 pu. When the grid voltage falls below 0.5 pu but not less than 0.1 pu, the converter could choose to achieve ride-through. To better study the transient performance of VSG under severe grid voltage sag, the grid voltage sags between 0.1 and 0.5 pu are studied in this paper.

Note that the main concerned problems of VSG in this paper are the transient angle instability, overcurrent and the violation of the grid code under grid voltage sag. Fortunately, the VSG control has two degrees of freedom. Thus, the simultaneous

$$E = \dfrac{K_q U_g(\alpha\sin\delta + \beta\cos\delta) - 1 + \sqrt{[K_q U_g(\alpha\sin\delta + \beta\cos\delta) - 1]^2 + 4\beta K_q(U_n + K_q Q_0)}}{2\beta K_q} \tag{5}$$

$$E = \frac{K_q U_g(\alpha\sin\delta + \beta\cos\delta) - \beta k_2 K_q - 1 + \sqrt{[K_q U_g(\alpha\sin\delta + \beta\cos\delta) - \beta k_2 K_q - 1]^2 + 4\beta K_q[(U_n + K_q Q_0) + k_2 K_q U_g(\alpha\sin\delta + \beta\cos\delta)]}}{2\beta K_q} \quad (7)$$

control for the phase angle and output current of VSG is theoretically feasible, which can be achieved by the combined control of APCL and RPCL, and thus the conflict among the three control objectives as mentioned in the introduction can be solved. For instance, though the increase of the reactive power reference alone goes against the current limitation, the reduction of the active power reference and the increase of the reactive power reference can be combined to enhance the transient angle stability of VSG while guaranteeing the current limitation under grid voltage sag. Similarly, to further control the reactive current of VSG for the demand of the grid code, the regulation in APCL and RPCL should be combined to meet the demand of the grid code for reactive current I_{q1}=1.0 pu under severe grid voltage sag [24] while the total current does not provoke the limit of 1.2 pu.

To achieve the above three control objectives without using the fault information, a dual-loop feedback control is presented in Fig. 1. The terminal voltage and reactive current of VSG are measured and feed back to APCL and RPCL with the feedback coefficients k_1, k_2 respectively, to regulate the phase angle and reactive current of VSG during fault. Note that the reactive current takes a large proportion in the output current of VSG under severe grid voltage sag. Thus, both the magnitude of the reactive current and the total current can be controlled by flexibly regulating coefficients k_1, k_2. In addition, only the terminal information of the converter is needed, which means the fault information acquisition is not required in the dual-loop feedback control. In addition, the mode switching is not necessary in the dual-loop feedback control since $(I_q - I_{q0})$ and $(E - U_n)$ are zero during normal state since the rated reactive current of VSG is generally set to I_{q0}=0 pu, and thus the two additional paths do not affect the normal operation of VSG. When the fault is occurred, $(I_q - I_{q0})$ and $(E - U_n)$ are not zero which means the feedback control in both APCL and RPCL is activated automatically.

To better analyze the transient performance of VSG when the dual-loop feedback control is applied, (5) is modified with the consideration of the dual-loop feedback control as (7).

Furthermore, the second order nonlinear differential equation of VSG in (6) with the dual-loop feedback control can be derived as

$$J\ddot{\delta} = -D\dot{\delta} + [(P_0 - P_e) - k_1(U_n - E)]$$
$$= -D\dot{\delta} + [(P_0 - (-\alpha U_g E(\theta_{vsg}, k_2)\cos\delta + \beta U_g E(\theta_{vsg}, k_2)\sin\delta$$
$$+ \alpha E(\theta_{vsg}, k_2)^2) - k_1(U_n - E(\theta_{vsg}, k_2))]$$
$$(8)$$

C. Modelling of the Paralleled System of VSG and VSC

In addition, the effectiveness of the dual-loop feedback control in a multiple-generators system should be considered as well. Note that the multiple generators can be aggregated with the order reduction method [30], [31]. Therefore, for the simplification but not losing the generality, a paralleled system of VSG and VSC with GFL control [32], [33] is studied in this paper. As shown in Fig. 2. C_{f2}, L_{f2}, Z_{T2} represent the capacitor and inductance of the filter, and the transformer's leakage

impedance of VSC. Z_1, Z_2 and Z_3 are the line impedances of the system. Different with VSG in Fig.1 which is connected to an ideal grid, the two converters in the paralleled system are connected to point of common coupling (PCC) whose voltage is fluctuated after fault, which can be expressed as $U_{pcc}\angle\theta_{pcc}$. The internal voltage of VSC is expressed as $U_0\angle\theta_{pll}$, where the phase angle of VSC is decided by PLL. The output currents of VSG and VSC are expressed as $I_1\angle(\theta_{vsg} + \varphi_{i1})$ and $I_2\angle(\theta_{pll} + \varphi_{i2})$, while φ_{i1}, φ_{i2} represent the angles of current phasor.
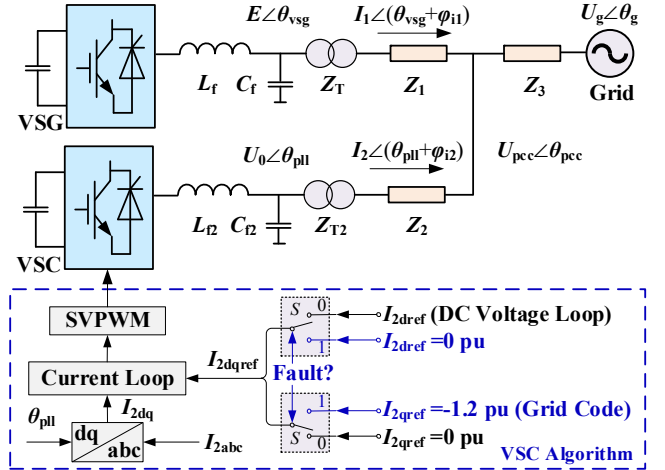

Fig. 2. Topology of the paralleled system of VSG and VSC with GFL control.

Note that the influence of the dc voltage and current loops of VSC can also be ignored during transient process since the transient angle stability of VSC is mainly determined by PLL [24], [31]. And the transient angle instability of VSC usually occurs due to the influence of the PLL dynamics under a severe grid voltage sag. Even so, the transient angle stability of VSG in the paralleled system and the effectiveness of the dual-loop feedback control for VSG are mainly focused in this paper. Thus, the transient process caused by PLL is not considered since the timescales between PLL and power loops of VSG are different [34], and thus the influence of the PLL dynamics on VSG is small. In addition, VSC is less likely to suffer the transient instability caused by PLL since the PCC voltage is supported by VSG to some degree during fault. With the above simplification of neglecting the PLL dynamics [33], VSC is represented as a controlled current source. And thus it can be considered that the output current of VSC is directly specified by the current references. Thereby, the large-signal model of the paralleled system of VSG and VSC can be reduced and simplified.

In addition, the output current magnitude and the current property of VSC have a great effect on VSG. To investigate this issue, the switching logic of VSC control in Fig. 2 is described as follows. When VSC operates during normal state, S is at the position of logical 0. The active current reference of VSC which generated by the dc voltage loop is about I_{2dref}=1.0 pu at rated active power while the reactive current reference is normally set as I_{2qref}=0. When a fault occurs, S is switched to 1. For the consideration of both the current limitation and grid

code [23], I_{2dref}=0 pu and I_{2qref}=-1.2 pu are required.

$$I_{2\,\text{dref}} = \begin{cases} 1.0 & \text{pu} \\ 0 & \text{pu} \end{cases}, \quad I_{2\,\text{qref}} = \begin{cases} 0 & \text{pu} \quad (S=0) \\ -1.2 & \text{pu} \quad (S=1) \end{cases} \quad (9)$$

where, I_{2d}, I_{2q} are the active current and reactive current of VSC, and φ_{i2}=arctan(I_{2q}/I_{2d}).

Thereafter, the voltage equation of VSC is derived as

$$U_0 e^{j\theta_{\text{pll}}} = a_3 E e^{j\theta_{\text{vsg}}} + a_1 U_g e^{j0} + (a_1 Z_3 + Z_2) I_2 e^{j(\theta_{\text{pll}} + \varphi_{i2})} \quad (10)$$

where, a_1= $Z_1/(Z_1+Z_3)$, a_3= $Z_3/(Z_1+Z_3)$, Z_2=R_2+jX_2, Z_3=R_3+jX_3.

Neglecting the PLL dynamics of VSC and then (10) can be decomposed in dq frame based on θ_{pll} as

$$\begin{cases} U_{0d} = U = a_3 E \cos\delta_{\text{pll}} + a_1 U_g \cos\theta_{\text{pll}} \\ \quad + a_1 (R_3 I_{2d} - X_3 I_{2q}) + (R_2 I_{2d} - X_2 I_{2q}) \\ U_{0q} = 0 = a_3 E \sin\delta_{\text{pll}} - a_1 U_g \sin\theta_{\text{pll}} \\ \quad + a_1 (R_3 I_{2q} + X_3 I_{2d}) + (R_2 I_{2q} + X_2 I_{2d}) \end{cases} \quad (11)$$

where, δ_{pll}=θ_{vsg}-θ_{pll}.

Similarly, the voltage equation of PCC is derived as

$$U_{\text{pcc}} e^{j\theta_{\text{pcc}}} = U_0 e^{j\theta_{\text{pll}}} - Z_2 I_2 e^{j(\theta_{\text{pll}} + \varphi_{i2})} \quad (12)$$

And (12) can be decomposed in dq frame based on θ_{pcc} as

$$\begin{cases} U_{\text{pcc}} \cos\delta_{\text{pcc}} = U_{\text{pll}} - (R_2 I_{2d} - X_2 I_{2q}) \\ U_{\text{pcc}} \sin\delta_{\text{pcc}} = -(R_2 I_{2q} + X_2 I_{2d}) \end{cases} \quad (13)$$

where, δ_{pcc}=θ_{vsg}-θ_{pcc}.

Thus, the large-signal model of the paralleled system of VSG and VSC can be built with $U_g \angle \theta_g$ in (8) replaced by $U_{\text{pcc}} \angle \theta_{\text{pcc}}$ in (9)-(13). And thus the influence of the output current property of VSC in the paralleled system on VSG can be analyzed based on the large-signal model. Note that when the transient performance of VSC in the paralleled system is further concerned, the PLL dynamics can be modelled again.

III. FEASIBLE COEFFICIENT REGION ANALYSIS

In this Section, the feasible coefficient region for the feedback coefficients of the dual-loop feedback control is analyzed and validated in both VSG and the paralleled system of VSG and VSC.

A. Feasible Coefficient Region of VSG

In the most of fault conditions, the dual-loop feedback control of VSG can achieve the transient angle stability, current limitation and demand of the grid code for the reactive current. Note that when the grid voltage further falls to less than 0.1 pu, the converter should trip immediately, while grid voltage falls above 0.5 pu need not to be controlled. However, when VSG faces a severe grid voltage sag about 0.1 pu, both APCL and RPCL may exceed their control margin, and then the control scheme may be ineffective. Therefore, the feasible coefficient region of the dual-loop feedback control of VSG with the grid voltage sags among 0.1~0.5 pu is analyzed in this paper. And the reasonable design for the feedback coefficients k_1, k_2 is necessary.

According to (8), the three control objectives can be achieved simultaneously based on the suitable feedback coefficients k_1, k_2 from APCL and RPCL. Thus, all of the sets of (k_1, k_2) which meet the control objectives are defined as the feasible

coefficient region of the control scheme. To obtain and analyze the feasible coefficient region can offer the guiding significance for the stable operation of VSG during fault.

To test the effectiveness of the dual-loop feedback control with different sets of (k_1, k_2), each set of (k_1, k_2) with the range from 0~3 pu is examined with step 0.01. And thus the feasible coefficient region of the dual-loop feedback control can be obtained. With the solution of (8), the transient performance of VSG can be depicted whether the control objectives are achieved or not with each set of (k_1, k_2). All of the 300*300 different sets of (k_1, k_2) are tested with the help of computer. After the examination, the feasible coefficient region of the control scheme is obtained. Note that the length of the 110 kV transmission line is normally between 50~80 km. Thus, two cases of VSG in Fig. 1, where the line lengths are 50 and 80 km under different grid voltage sags are tested with the parameters of VSG shown in Table II.
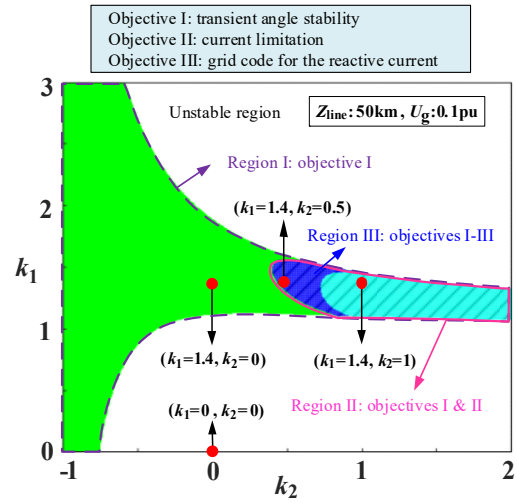

Fig. 3. Feasible coefficient region of the dual-loop feedback control in case 1: U_g=0.1 pu.

TABLE II
PARAMETERS OF VSG

Parameters	Value	Parameters	Value
P_0	100 MW (1.0 pu)	ω_n	100π rad/s
Q_0	0	Z_T	0.005 pu
J	0.3 pu	L_f	0.2 pu
D	1 pu	C_f	0.15 pu
K_q	0.05 pu	r_1	0.2542 Ω/km
E_0	690 V	l_1	$2.287e^{-3}$ H/km
U_g	110 kV	c_1	$5.214e^{-9}$ F/km

In case 1, the line length is set to 50 km. The grid voltage sag occurs at t=0.5 s and recovers at t=1.5 s. To better analyze the characteristics of the feasible coefficient region, the fault degrees when the grid voltage falls among 0.1~0.4 pu are examined.

The feasible coefficient region of the dual-loop feedback control is described and explained in detail by taking case 1 under U_g=0.1 pu as an example. As shown in Fig. 3, the feasible coefficient region is divided into four areas with different colors including white, green, light blue and dark blue. Firstly, the unstable region equals to the white area, where the phase angle of VSG is not stable during fault with the related sets of (k_1, k_2) within the white area. Secondly, Region I containing the green, light blue and dark blue areas represents the stable operating region where the phase angle of VSG is

stable during fault with the related sets of (k_1, k_2). However, the other two control objectives including the current limitation and the requirement of the grid code for the reactive current cannot

be achieved in the green area. Furthermore, in Region II which consists of the light blue and dark blue areas, both the transient angle stability and the current limitation can be achieved. But
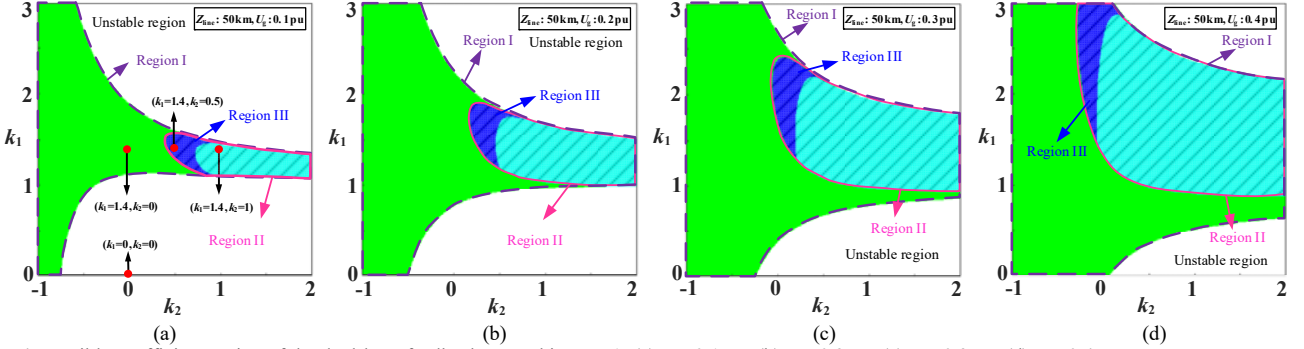

Fig. 4. Feasible coefficient region of the dual-loop feedback control in case 1: (a) U_g=0.1 pu. (b) U_g=0.2 pu. (c) U_g=0.3 pu. (d) U_g=0.4 pu.
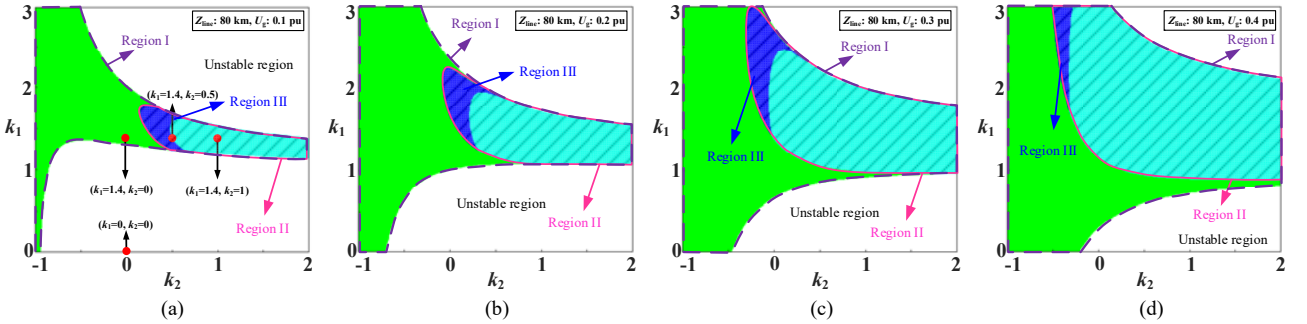

Fig. 5. Feasible coefficient region of the dual-loop feedback control in case 2: (a) U_g=0.1 pu. (b) U_g=0.2 pu. (c) U_g=0.3 pu. (d) U_g=0.4 pu.
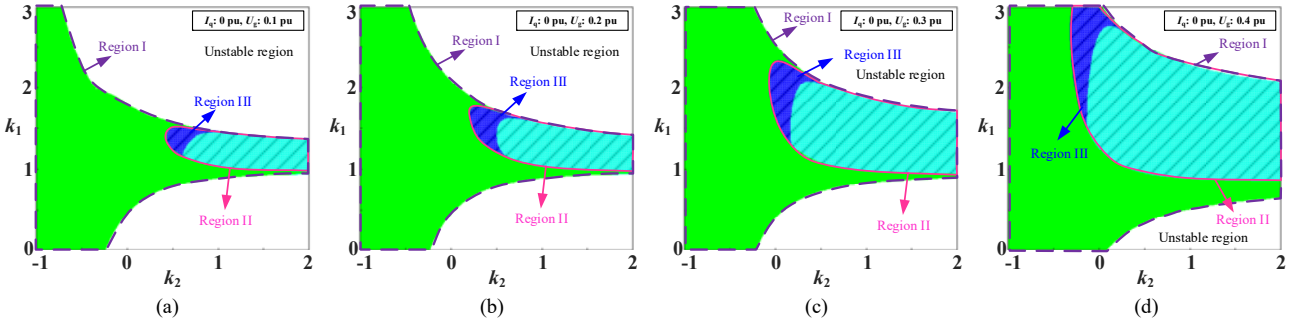

Fig. 6. Feasible coefficient region of the dual-loop feedback control in case 3: (a) U_g=0.1 pu. (b) U_g=0.2 pu. (c) U_g=0.3 pu. (d) U_g=0.4 pu.
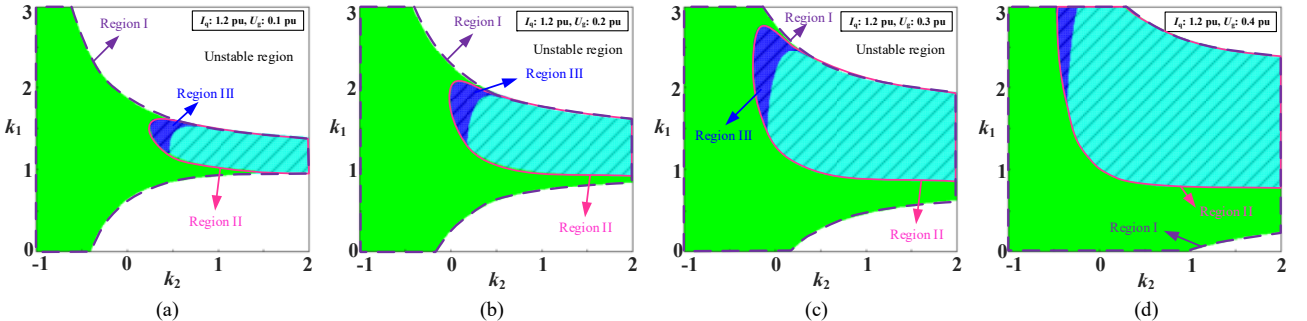

Fig. 7. Feasible coefficient region of the dual-loop feedback control in case 4: (a) U_g=0.1 pu. (b) U_g=0.2 pu. (c) U_g=0.3 pu. (d) U_g=0.4 pu.

the requirement of the grid code is not guaranteed in the light blue area. Last but not least, only in Region III which equals to the dark blue area can all of the three control objectives be guaranteed simultaneously with the related sets of (k_1, k_2).

Obviously, the change of the areas from white, green, light blue to dark blue area is corresponding to the progressive realization of the three control objectives.

As shown in Fig. 4(a)~(d), with the deeper grid voltage sags from 0.4 to 0.1 pu in case 1, the shading area of the feasible coefficient region with the same color becomes smaller. For example, the areas of Region I, II and III in Fig. 4(a) are smaller than that of Fig. 4(b). Note that even if the fault is severe when the grid voltage falls to 0.1pu, there still exists a dark blue area (Region III) where all of the three control objectives can be achieved.

In case 2, to further validate the existence of the feasible coefficient region under the worse condition, the line length in Fig. 1 is increased to 80 km. The grid voltage sag occurs at t=0.5 s and recovers at t=1.5 s. As shown in Fig. 5, the change rule of the areas with the different colors under the variety of the grid voltage sags in case 2 is the same as it in case 1. As a comparison, the shading area with the same color in case 2 becomes smaller compared with them in case 1 since the fault condition is worse caused by the longer line. Nevertheless, since the dark blue area (Region III) still exists even through the grid voltage falls to 0.1 pu in case 2 with the longer line, the universality of the dual-loop feedback control is guaranteed.

According to the analysis of case 1 and case 2, it can be found that the large k_2 is helpful for the current limitation but harmful for the transient angle stability. In addition, the large k_1 improves the transient angle stability while limiting the output current. With the flexible configuration of (k_1, k_2), the control objectives of the transient angle stability, current limitation, and the requirement of the grid code for the reactive current can all be achieved. In addition, the dark blue area (Region III) which meets all of the three control objectives is moved exponentially from upper left to lower right with the deeper grid voltage sag in each case.

B. Feasible Coefficient Region of the Paralleled System

Thereafter, the effectiveness of the dual-loop feedback control for VSG in the paralleled system of VSG and VSC is considered. Similarly, the feasible coefficient region of the paralleled system is obtained based on the large-signal model derived in Section II-C. Thereafter, two cases of the paralleled system in Fig.2, where the reactive current references of VSC are 0 pu and -1.2 pu under different grid voltage sags are tested with the parameters of the paralleled system shown in Table III.

In case 3, I_{2qref} of VSC during fault is set to 0 pu, where the demand of the grid code for VSC is not considered. The grid voltage sag occurs at t=0.5 s and recovers at t=1.5 s. Similarly, the feasible coefficient region under the grid voltage sags among 0.1~0.4 pu is depicted in Fig. 6.

In case 4, I_{2qref} of VSC during fault is set to -1.2 pu, which is based on the configuration in (9). And the related feasible coefficient region is shown in Fig. 7.

TABLE III
PARAMETERS OF THE PARALLELED SYSTEM

Parameters	Value	Parameters	Value
P_{vsg}/P_{vsc}	100/100 MW	U_g	110 kV
Q_{vsg}/Q_{vsc}	0/0 MW	Z_T/Z_{T2}	0.005/0.005 pu
J	0.3 pu	L_f/L_{f2}	0.2 pu
D	2 pu	C_f/C_{f2}	0.15 pu
K_q	0.2 pu	Length of Z_1	30 km
E	690 V	Length of Z_2	20 km
U_0	690 V	Length of Z_3	10 km

Obviously, the change rule of the areas with the different colors under the variety of the grid voltage sags in case 3 and case 4 is the same as it in case 1 and case 2. That is, the shading areas with different colors becomes smaller with the deeper grid voltage sag. As a comparison, the shading areas with the same color in case 3 are smaller than that in case 4 due to the influence of the reactive current of VSC. When the current property of VSC tends to reactive instead of active, the feasible coefficient region of the control scheme becomes larger. Thus, the reactive current of VSC is helpful for the control objectives of VSG in the paralleled system under grid voltage sag.

C. Validation of the Feasible Coefficient Region Analysis

The feasible coefficient region analysis is validated by testing the effectiveness of the dual-loop feedback control with the specific sets of (k_1, k_2) in the areas with different colors. The worst fault condition of VSG such as U_g=0.1 pu in case 2 is validated. Taking four sets of (k_1, k_2) in each area with different colors as examples, which are $(k_1=0, k_2=0)$, $(k_1=1.4, k_2=0)$, $(k_1=1.4, k_2=0.5)$, $(k_1=1.4, k_2=1)$.

Note that the analytic solution of (8) is hard to obtain. Instead, a graphical solution such as the phase portrait can provide a simple and intuitive result. Thus, the feasible coefficient region of VSG is first validated by the phase portrait method. Since the output current of VSG is one of the control objectives, a 3-D phase portrait with $\dot{\delta} - \delta - I$ is depicted in Fig. 8. By comparing Fig. 8(a) and (b), when $(k_1=0, k_2=0)$ is applied, the phase angle of VSG is divergent, which means VSG loses the transient angle stability while the current provokes the limit value of 1.2 pu. As a comparison, when $(k_1=1.4, k_2=0.5)$ is applied, the phase angle of VSG is convergent and current limitation of 1.2 pu is guaranteed, which means the transient angle stability and current limitation are achieved with the reasonable set of (k_1, k_2).
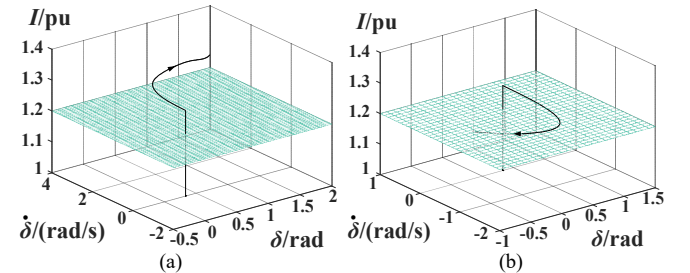

Fig. 8. 3-D phase portrait with the dual-loop feedback control during fault in case 2: (a) $k_1=0, k_2=0$. (b) $k_1=1.4, k_2=0.5$.

Although the phase portrait is intuitive, the characteristics such as magnitude of the reactive current cannot be reflected. Thus, the conclusion needs to be further validated by simulation carried out in MATLAB/Simulink. Fig. 9 shows the dynamics of VSG during the transient process in case 2 with four sets of (k_1, k_2) as mentioned. As shown in Fig. 9(a), when $(k_1=0, k_2=0)$ in the white area is applied, which means the control is not applied, the phase angle of VSG is divergent and the current provokes the limit. The simulation result coincides with Fig. 8(a). As shown in Fig. 9(b), when $(k_1=1.4, k_2=0)$ in the green area of Region I is applied, the phase angle of VSG is convergent, but the current still provokes the limit of 1.2 pu. As shown in Fig. 9(c), with $(k_1=1.4, k_2=1)$ in the light blue area of

Region II, VSG can reach a stable equilibrium point while the current limitation is also guaranteed. However, the requirement of the grid code for the reactive current is not achieved. As a comparison in Fig. 9(d), only with (k_1=1.4, k_2=0.5) in Region III can the transient angle stability, current limitation, and demand of the reactive current all be achieved, which coincides
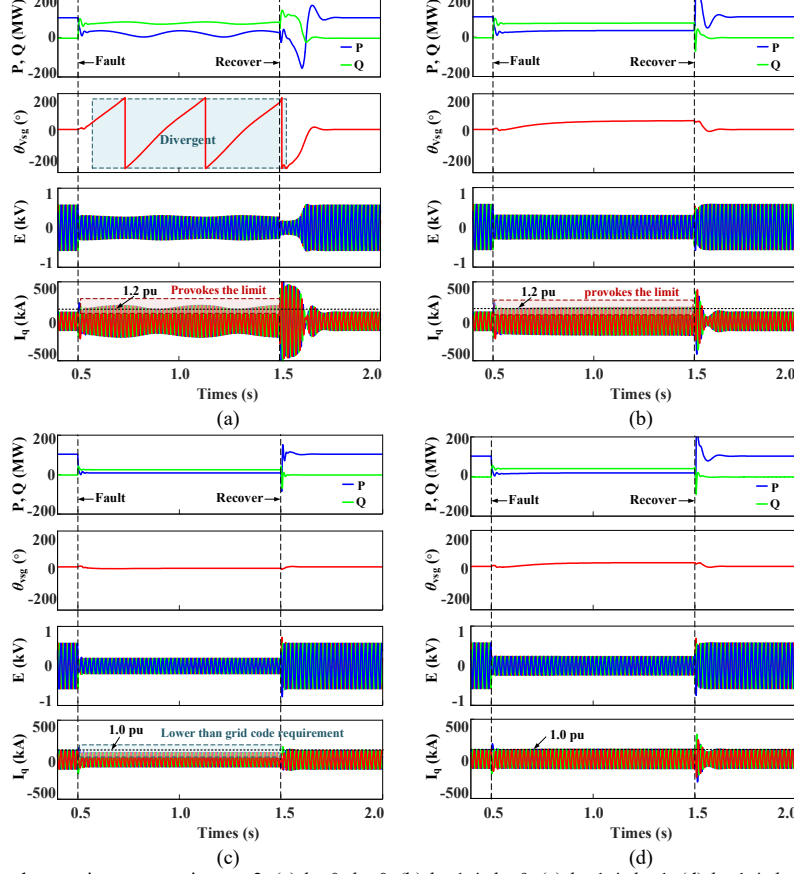

Fig. 9. Dynamics of VSG during the transient process in case 2: (a) k_1=0, k_2=0. (b) k_1=1.4, k_2=0. (c) k_1=1.4, k_2=1. (d) k_1=1.4, k_2=0.5.
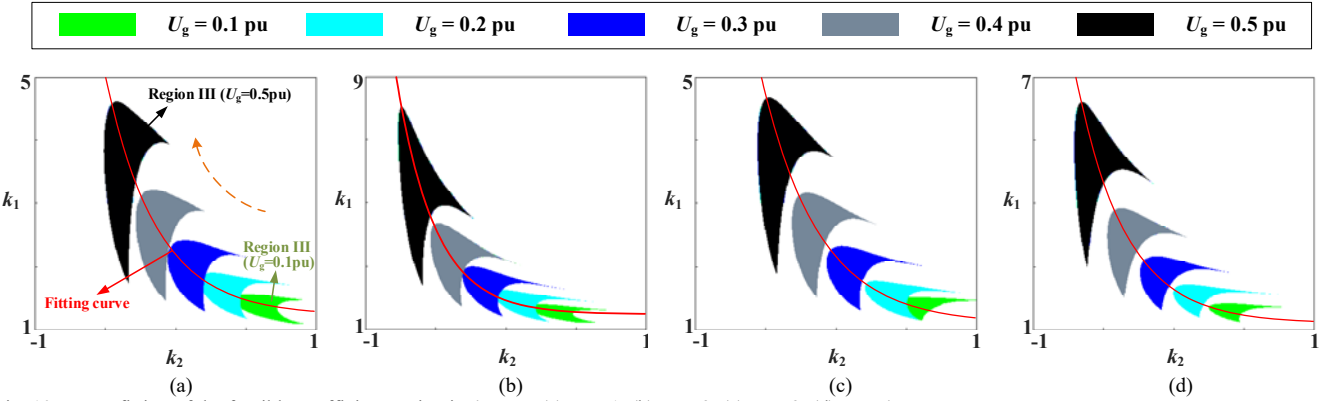

Fig. 10. Curve fitting of the feasible coefficient region in 4 cases: (a) case 1. (b) case 2. (c) case 3. (d) case 4.

with Fig. 8(b).

Overall, the effectiveness of the dual-loop feedback control with the sets of (k_1, k_2) in the different areas can be validated.

IV. A DUAL-LOOP ADAPTIVE FEEDBACK CONTROL

In this Section, the curve fitting of the feasible coefficient region is applied to obtain the reasonable functional relationship between the feedback coefficients. Then an additional reactive power feedback loop is proposed to realize the self-adaptive regulation of the feedback coefficients.

A. Curve Fitting of the Feasible Coefficient Region

The feasible coefficient region analysis of 4 cases in Fig. 4 to Fig. 7 in Section III offers the reference for the selection of the feedback coefficients (k_1, k_2) of the dual-loop feedback

control. Therefore, the general conclusion and guidelines for the selection of the feedback coefficients can be summarized as follows:

1) Region I, II and III are the feasible coefficient regions corresponding to different control objectives. Only in Region III which equals to the dark blue area with the related sets of (k_1, k_2) can all of the three control objectives of VSG be guaranteed.

2) The areas of Region I, II and III become smaller with the deeper grid voltage sags. As for VSG with a transmission line between 50~80 km, the longer line length leads to the larger area of Region III. As for the paralleled system, when the output current property of VSC tends to be reactive from active, the area of Region III of VSG becomes larger.

3) Larger k_2 leads to the larger output current and the worse transient angle stability of VSG, while larger k_1 leads to the better transient angle stability and smaller output current of VSG. Region III is made up with the reasonable co-regulation of k_1 and k_2.

4) With the deeper grid voltage sag, Region III in each case is moved exponentially from upper left to lower right.

Although the general guidelines for the selection of the feedback coefficients is summarized, it is still a kind of hindsight after knowing the fault information. The real-time regulation of the feedback coefficients with the fault degrees cannot be realized. Therefore, a self-adaptive regulation of (k_1, k_2) needs to be investigated. First the functional relationship between k_1 and k_2 should be found.

The article 4 of the general guidelines is applied: Region III in each case is moved exponentially from upper left to lower right with the deeper grid voltage sag. To better analyze the change rule, Region III under grid voltage sags among 0.1 to 0.5 pu in each case can be plotted in the same figure.

As shown in Fig. 10, obviously, there is an upward and leftward bulge in each area under deeper grid voltage sags, and the connection to all of the endpoints coincides with the exponential curve. Therefore, with the change rule, the fitting curve of the feasible coefficient region in each case can be obtained easily with the help of Cftool (Curve Fitting Toolbox) of Matlab.

$$k_1 = ae^{-bk_2} + c \qquad (14)$$

where, a, b, c are the fitting parameters. And they have the unique value in each case. According to (14), the functional relationship between k_1 and k_2 can be derived, which is expressed as $k_1=F(k_2)$.

Subsequently, the parameter fitting in (14) can be obtained with the help of Cftool as well. As shown in Table IV, the parameters with the subscripts 1~4 represent the related fitting parameters of case 1~4.

TABLE IV
PARAMETERS OF THE FITTING CURVES IN 4 CASES

Parameters	Value	Parameters	Value
a_1	0.9891	a_3	1.081
b_1	2.72	b_3	2.443
c_1	1.216	c_3	1.1
a_2	0.4453	a_4	0.8216
b_2	3.61	b_4	2.838
c_2	1.448	c_4	1.16

Note that the system information in a specific case for the parameter fitting can be obtained in advance before fault, such as the system topology and line length. Thereby, the feasible

coefficient region analysis can be carried out and the functional relationship between k_1 and k_2 can also be predetermined before fault in each case. Therefore, as for a certain case under the grid voltage sags among 0.1 to 0.5 pu, there is always a set of (k_1, k_2) in the fitting curve where all of the three control objectives of VSG after fault can be achieved.

B. Adaptive Feedback Control Based on an Additional Reactive Power Feedback Loop

According to (14), the feedback coefficient k_1 can be expressed by k_2. To further achieve the self-adaptive regulation of (k_1, k_2) related to the fault degrees, the relationship between k_2 and the grid voltage sag should be found.

Thus, a dual-loop adaptive feedback control is proposed based on an additional reactive current feedback loop to achieve the self-adaptive regulation of k_2 under different grid voltage sags. For example, the requirement of the grid code for the reactive current of VSG during fault is I_{q1}=1.0 pu. Then the additional reactive current feedback loop is added as shown in the red block in Fig. 11, which is regarded as the Q feedback loop 2 with I_{q1}, while the initial feedback path is the Q feedback loop 1 with the rated reactive current I_{q0}=0 pu. With the Q feedback loop 2, k_2 is derived adaptively to achieve the demand of the reactive current, and to further regulate the active and reactive power references by the Q feedback loop 1 and P feedback loop respectively. k_{20} is the initial value of k_2, which is chosen as the maximum value of k_2 in the worst fault condition of VSG such as U_g=0.1 pu in each case. Besides, k_2 is obtained before a saturation block, whose upper and lower limits are corresponding to the maximum and minimum values of k_2 in the fitting curve in each case.
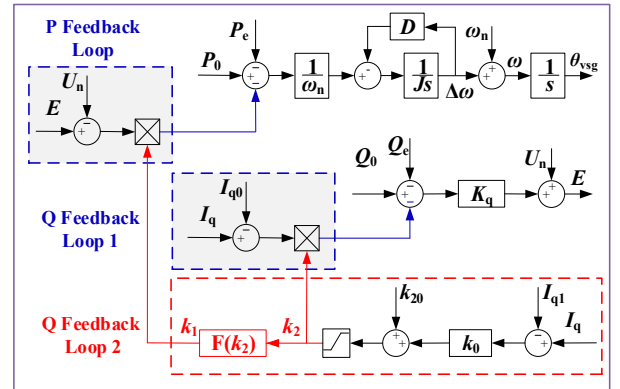

Fig. 11. The dual-loop adaptive feedback control of VSG with an additional reactive power feedback loop.

In Fig. 11, the dual-loop adaptive feedback control based on an additional reactive power feedback loop is presented, which is also depicted in the red block in Fig. 1. The realization of the proposed control scheme is explained as follows. With the feasible coefficient region analysis in Section III, Region II which meets the two control objectives of the transient angle stability and the current limitation is shrunken with the deeper grid voltage sag in each case. And Region II under the deeper grid voltage sag is a complete subset of Region II under the shallower grid voltage sag.

Thus, first k_2 is chosen as the upper limit of the fitting curve in the worst fault condition of VSG such as U_g=0.1 pu in a certain case. When the grid voltage sags are changed from 0.1

to 0.5 pu, the proposed control scheme with the feedback coefficients k_2 and the related $k_1=F(k_2)$ in the fitting curve can always achieve the transient angle stability and the current limitation. Second, in the Q feedback loop 2, the perception of the fault degrees is realized indirectly due to the difference between I_q and the set value I_{q1}, and then k_2 can be derived to further regulate the reactive power reference and thus the demand of the reactive current can be achieved. Obviously, a k_2 for the demand of the reactive current combining with the related $k_1=F(k_2)$ in the fitting curve constitutes a set of (k_1, k_2), which can achieve the control objectives of transient angle stability, current limitation and requirement of the grid code for the reactive current at the same time.

In addition, the upper limit and lower limit of k_2 is controlled by the saturation block, which ensures that the derived k_2 is within the region under the grid voltage sags among 0.1 to 0.5 pu in each case. Note that the feedback coefficient k_0 of the Q feedback loop 2 is normally designed among 100~300 based on the practical experience, where the high regulating speed and accuracy can be realized while the noise and oscillation can be avoided.

Therefore, with the proposed control scheme, the three control objectives can all be achieved since the feedback coefficients (k_1, k_2) are within the feasible coefficient region due to the self-adaptive regulation.

C. Root Locus Analysis

In addition, the root locus of VSG with the proposed control scheme during fault can also be pre-analyzed to ensure the stability and the tuning of the control loops [35]. Taking case 2 with the grid voltage sags from 0.5 to 0.1 pu as an example, the dominant mode ($\Delta\theta_{vsg}$) trajectory of VSG during fault is shown in Fig. 12. It can be found that the root locus related to the fault degrees is still far away from the imaginary axis when the grid voltage decreases to 0.1 pu, which means the stability margin of VSG with the proposed dual-loop adaptive feedback control is large enough. Even if the control loops are unstable, the feedback coefficients in specific case can be redesigned before fault based on the pre-analyzed result. Thus, the stability and tuning of the control loops of VSG can be guaranteed.
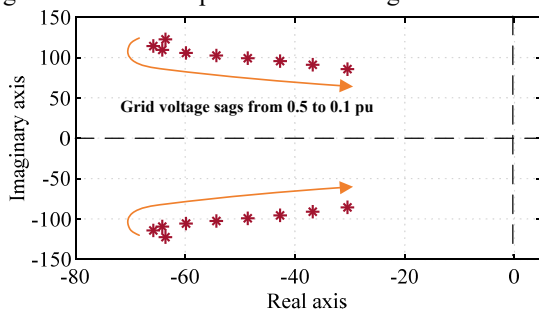

Fig. 12. Dominant mode trajectory of VSG (Grid voltage sags from 0.5 to 0.1pu) during the transient process in case 2.

V. CASE STUDIES

In this Section, the validation of the proposed control scheme in both VSG and the paralleled system of VSG and VSC is carried out by case studies. The robustness to the parameter errors and the comparison with the method based on the fault information are discussed as well.

A. Validation Under a VSG System

To analyze the effectiveness of the proposed control scheme, case 2 of VSG and case 3 of the paralleled system are validated as examples in MATLAB/Simulink. The method in [12], which is an adaptive mode-switching control, is also analyzed as a comparison.

In case 2, the proposed control scheme for VSG is validated. The line length is set to 80 km. The grid voltage falls to 0.15 pu and 0.45 pu respectively at t=0.5 s and recovers at t=1.5 s. k_0 is set to 300. The system parameters are shown in Table II.

Fig. 13 shows the dynamics of VSG during the transient process in case 2 under U_g=0.15 pu with or without the control. As shown in Fig. 13(a), when the proposed control scheme is not applied, the phase angle of VSG is divergent and the current provokes the limit. In Fig. 13(b), although VSG does not lose the synchronization, the phase angle and power oscillate in a bounded manner due to the mode-adaptive control in [12]. Besides, the fault current of VSG provokes the limit of 1.2 pu periodically with this method. As a comparison in Fig. 13(c), when the proposed control scheme is applied, a set of the self-adaptive coefficients (k_1=1.76, k_2=0.27) are derived. Thus, the phase angle of VSG is convergent, and the reactive current is controlled to the set value 1.0 pu while the current does not provoke the limit of 1.2 pu.

Fig. 14 shows the dynamics of VSG during the transient process in case 2 under U_g=0.45 pu with or without the control. As shown in Fig. 14(a), when the proposed control scheme is not applied, the phase angle of VSG is still divergent even if the grid voltage sag is shallower. In Fig. 14(b), the mode-adaptive control could not activate timely since the fault is slight and thus the effectiveness to control the phase angle is small. As a comparison in Fig. 14(c), when the proposed control scheme is applied, a set of the self-adaptive coefficients (k_1=5.23, k_2=-0.47) are derived. Thus, the transient angle stability, current limitation, and demand of the reactive current of VSG can all be achieved. Therefore, the effectiveness of the proposed control scheme for VSG is validated.

B. Validation Under the Paralleled System

In case 3, the proposed control scheme for the paralleled system of VSG and VSC is validated. The grid voltage falls to 0.15 pu and 0.45 pu respectively at t=0.5 s and recovers at t=1.5 s. I_{2qref} of VSC remains 0 pu during fault, which is harmful to the control objectives of VSG. k_0 is set to 150. The system parameters are shown in Table III.

Fig. 15 shows the dynamics of VSG in the paralleled system during the transient process in case 3 under U_g=0.15 pu with or without the control. As shown in Fig. 15(a), when the proposed control scheme is not applied, the phase angle of VSG is divergent and the current provokes the limit. In Fig. 15(b), the phase angle and current still oscillate periodically. As a comparison in Fig. 15(c), when the proposed control scheme is applied, a set of the self-adaptive coefficients (k_1=1.38, k_2=0.52) are derived. Thus, all of the three control objectives of VSG can be achieved.

Fig. 16 shows the dynamics of VSG in the paralleled system during the transient process in case 3 under U_g=0.45 pu with or without the control. As shown in Fig. 16(a), when the proposed control scheme is not applied, the phase angle of VSG is increased but not divergent due to the shallower grid
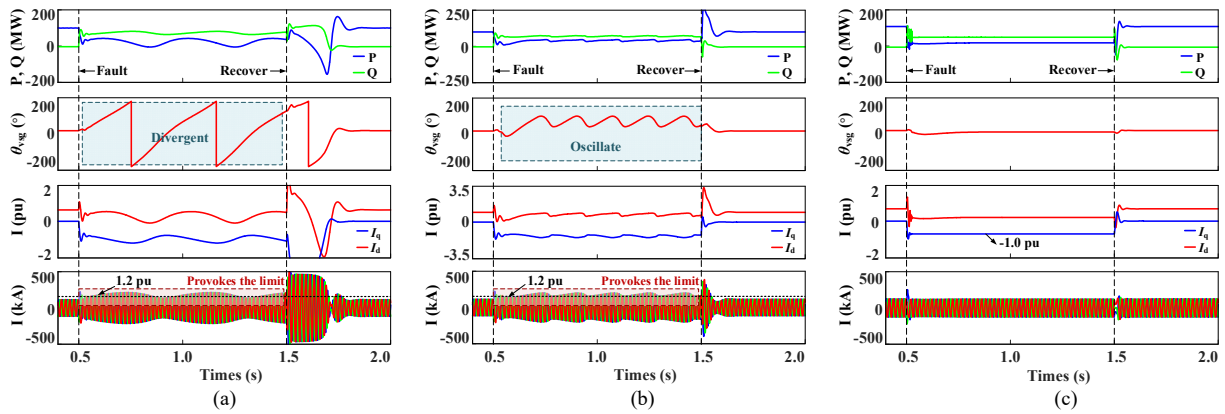
Fig. 13. Dynamics of VSG during the transient process in case 2 under U_g=0.15 pu: (a) without control. (b) with control in [12]. (c) with the proposed control.
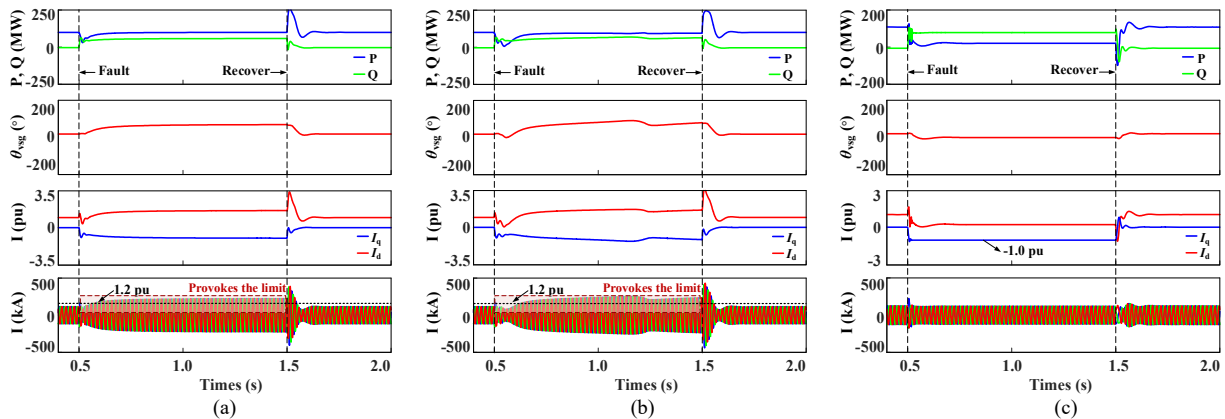

Fig. 14. Dynamics of VSG during the transient process in case 2 under U_g=0.45 pu: (a) without control. (b) with control in [12]. (c) with the proposed control.
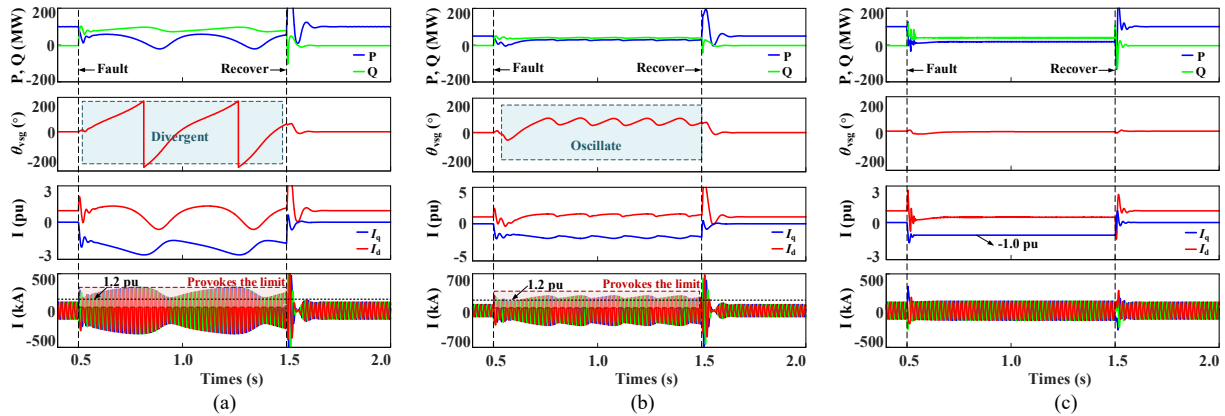

Fig. 15. Dynamics of VSG during the transient process in case 3 under U_g=0.15 pu: (a) without control. (b) with control in [12]. (c) with the proposed control.
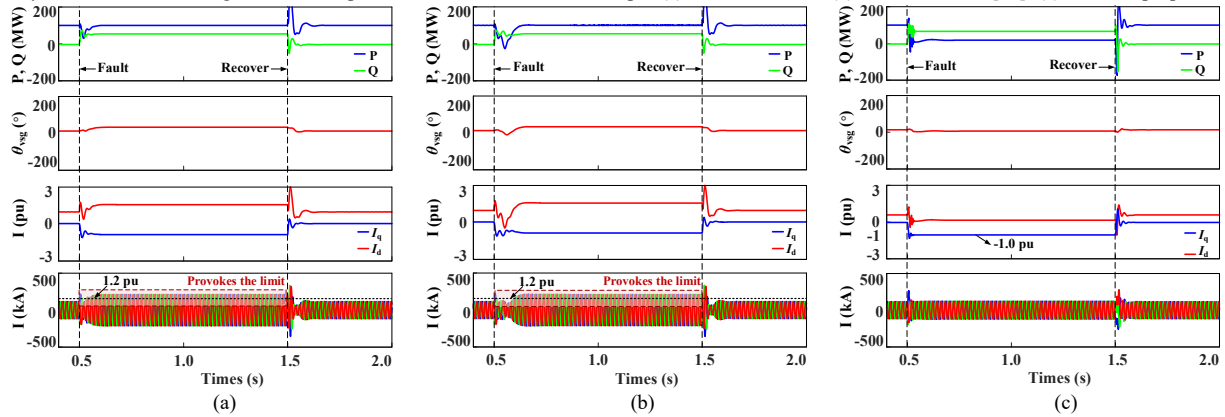

Fig. 16. Dynamics of VSG during the transient process in case 3 under U_g=0.45 pu: (a) without control. (b) with control in [12]. (c) with the proposed control.
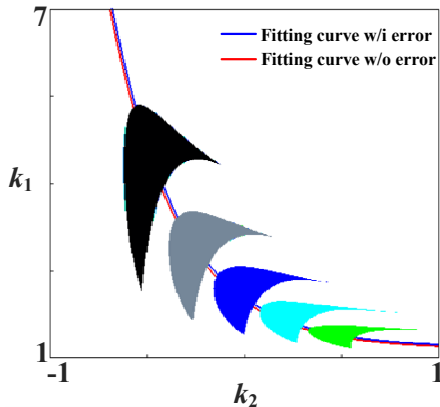
Fig. 17. Curve fitting of the feasible coefficient region in cases 4 with or without the error of the line length.

voltage sag. However, the current is increased until the limit is provoked. In Fig. 16(b), the mode-adaptive control could not even activate since the fault is slight and the phase angle is stable. But the current limit is provoked as the same as that in Fig. 16(a). As a comparison in Fig. 16(c), when the proposed control scheme is applied, a set of the self-adaptive coefficients (k_1=2.99, k_2=0.23) are derived. Similarly, all of the three control objectives for VSG in the paralleled system are achieved as well.

In short, with the dual-loop adaptive feedback control, the self-adaptive regulation of the feedback coefficients (k_1, k_2) of VSG can be achieved, and thus the transient angle stability, current limitation and the requirement of the grid code for the reactive current of VSG can be achieved simultaneously. And the effectiveness of the proposed control scheme is validated in both VSG and the paralleled system.

C. Robustness to the Parameter Errors

In practice, there are some inevitable errors of the system parameter adopted in the control loops, which may be harmful to the effectiveness of the proposed control scheme. Therefore, the robustness to the parameter errors should be considered. In special, the parameter error due to the length measurement of the transmission line is a primary error source of the proposed control scheme, which should be discussed.

To analyze the influence of the parameter errors caused by the length measurement on the proposed control scheme, the paralleled system in case 4 with the error of the line length is studied as a comparison. The line lengths of Z_1, Z_2 and Z_3 are measured as 27 km, 18 km and 9 km, which exist a relatively large error of 10% compared with the precise parameters shown in Table IV. Thereby, with the parameter errors adopted in the control loops, the related fitting curve of the feasible coefficient region in case 4 is also influenced. According to Section IV-A, the fitting parameters of the fitting curve in case 4 are changed as a_3'=1.081, b_3'=2.443, c_3'=1.1 from their original values shown in Table IV. The comparison between the original fitting curve in case 4 and the fitting curve influenced by the error of the line length is depicted in Fig. 17.

As shown in Fig. 17, the red curve is the original fitting curve in case 4 which is also plotted in Fig. 10(d), while the blue curve is the fitting curve with the error of the line length. Obviously, there is only a small derivation between the two

curves, which means the further self-adaptive regulation of (k_1, k_2) is almost unaffected by the error of the line length.

To verify the robustness of the proposed control scheme to the parameter errors, the dynamics of the paralleled system during the transient process in case 4 with or without a 10% error of the line length are depicted in Fig. 18. The grid voltage falls to 0.15 pu at t=0.5 s and recovers at t=1.5 s. I_{2qref} of VSC is set to -1.2 pu during fault, which is helpful to the control objectives of VSG. k_0 is set to 150. Other system parameters remain unchanged.

When the proposed control scheme is not applied, the transient angle stability, current limitation and the requirement of the grid code for VSG are not guaranteed in Fig. 18(a), while all of the three control objectives are achieved in Fig. 18(b) with the proposed control scheme. As a comparison, when a 10% error of the line length is adopted in the control loops, the self-adaptive coefficients are changed as (k_1=1.38, k_2=0.52) from their precise values (k_1=1.35, k_2=0.51) without the error. Although there is a mismatch of the self-adaptive feedback coefficients caused by the error of the line length, it only has a little impact on the control performance since the area of the feasible coefficient region in Fig. 17 is large enough for a little change of the fitting curves. As expected in Fig. 18(c), the proposed control scheme is still effective at the cost of a little larger fluctuation of the variables due to the error.

In short, the area of the feasible coefficient region of the proposed control scheme is large enough for the achievement of the three control objectives. Thus, the robustness of the proposed control scheme to the parameter errors such as the error of the line length is guaranteed.

D. Comparison with the Method Based on Fault Information

Note that the proposed control scheme can be utilized without using fault information, while the method based on the fault information acquisition may be not effective when the fault detecting device is not available. Even so, the performance of the method with the fault information should be examined as a comparison. Therefore, the method in [27], which is a parameter-switching control based on the fault information, is also examined as a comparison.

Case 2 in Section V-A is analyzed again in Fig. 19 with both the proposed control scheme and the method in [27]. The grid voltage falls to 0.3 pu at t=0.5 s and recovers at t=1.5 s. k_0 is set to 300. Other system parameters remain unchanged.

As shown in Fig. 19(a), the control objectives of VSG are not achieved without control. In Fig. 19(b), the transient angle stability and the current limitation of VSG are guaranteed with the parameter-switching control based on the fault information. And the fault information acquisition leads to good control performance. However, the requirement of the grid code for the reactive current of VSG is not realized in the method [27] since I_q is about 0.9 pu in Fig. 19(b). As a comparison in Fig. 19(c), when the proposed control scheme is applied, a set of the self-adaptive coefficients (k_1=2.12, k_2=-0.12) are derived, and all of the three control objectives can be achieved as well.

Obviously, the performance of the proposed control scheme is almost equal to the method based on the fault information. Therefore, the hardware requirement of the proposed control scheme is low while the performance remains high level.
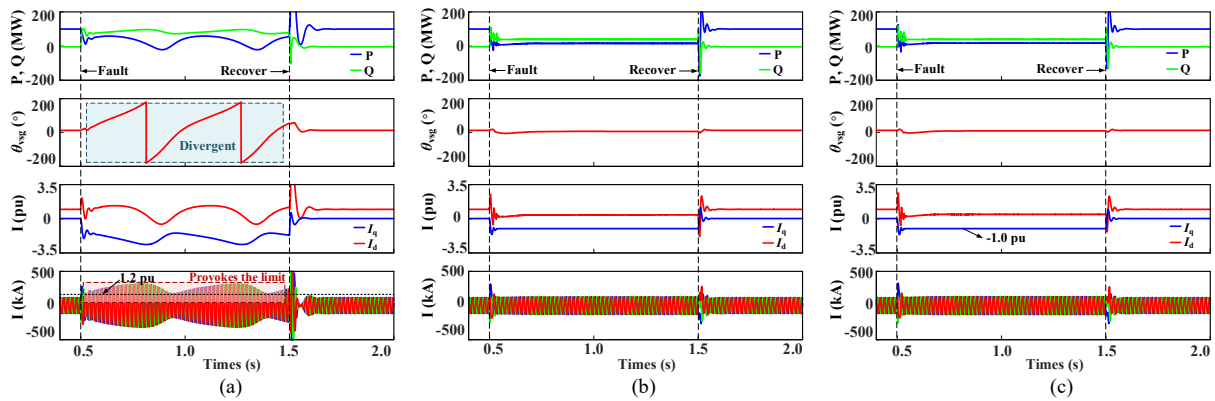
Fig. 18. Dynamics of VSG during the transient process in case 4 under U_g=0.15 pu with a 10% error in the line length: (a) without control. (b) with control in [12]. (c) with the proposed control.
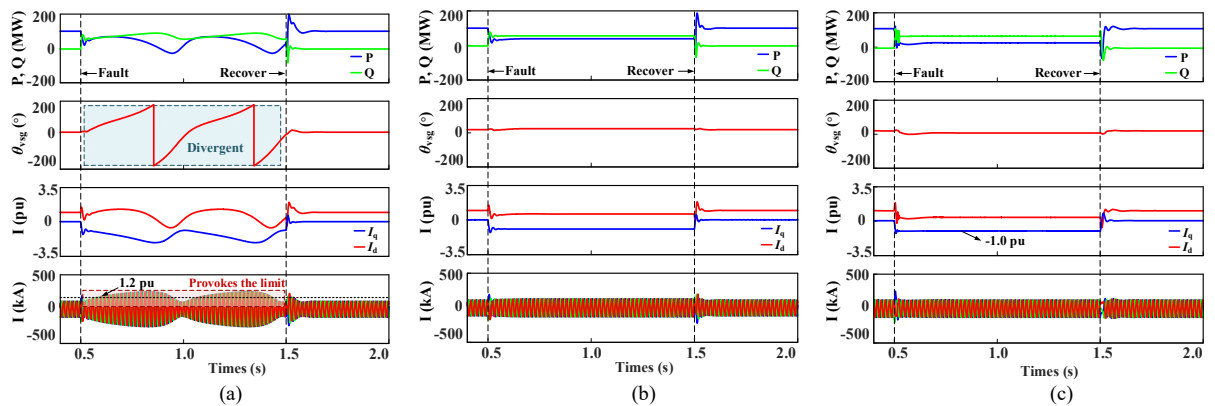

Fig. 19. Dynamics of VSG during the transient process in case 2 under U_g=0.3 pu: (a) without control. (b) with control based on the fault information in [27]. (c) with the proposed control.
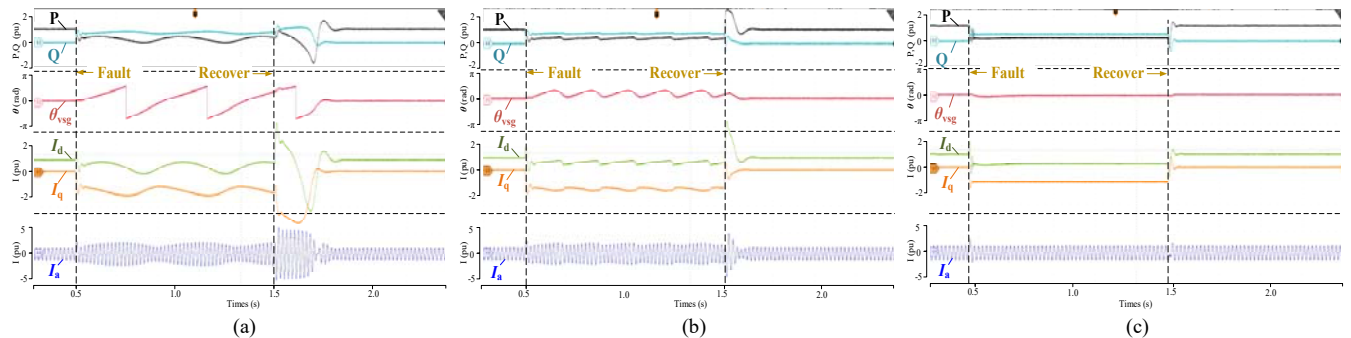

Fig. 21. Experimental results of VSG during the transient process in case 2 under U_g=0.15 pu: (a) without control. (b) with control in [12]. (c) with the proposed control.
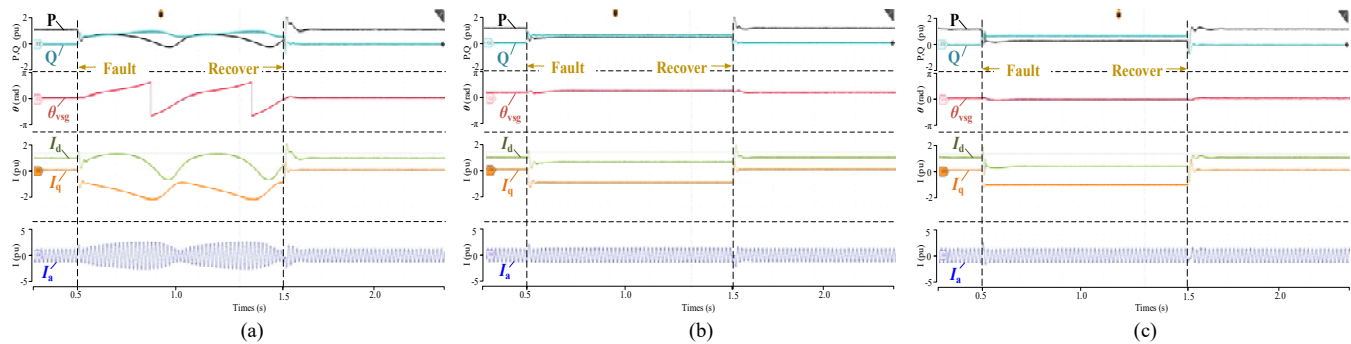

Fig. 22. Experimental results of VSG during the transient process in case 2 under U_g=0.3 pu: (a) without control. (b) with control based on the fault information in [27]. (c) with the proposed control.
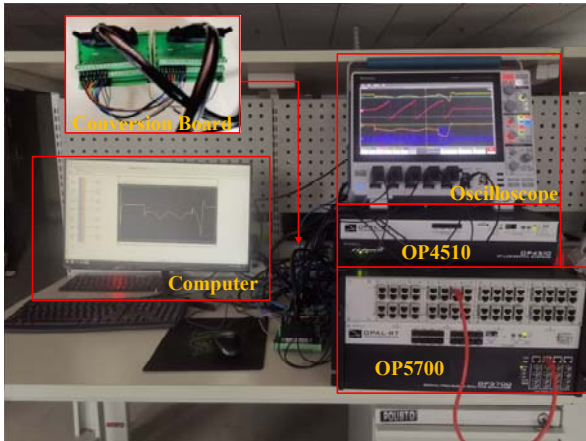
Fig. 20. OPAL-RT real-time simulation platform.

VI. Experimental Results

To further verify the effectiveness of the proposed control scheme and the simulation results, the experimental validation is carried out based on the OPAL-RT real-time simulation platform. The configuration diagram and physical picture of the experimental platform are shown in Fig. 20. The main system of VSG is modeled in the OP5700 simulator while the dual-loop adaptive feedback control is implemented in the OP4510 simulator. The signal transmission between the main system and control system in the real-time situation is realized by the conversion board. The software code is generated by the real-time WorkShop under a MATLAB/Simulink environment.

The advantages of the experiment based on the OPAL-RT real-time simulation platform compared with the simulation are mainly as follows: 1) the uncertain measurement disturbances and the unknown harmonics in the signal transmission cables and the device can be accurately reflected in the experimental results instead of the simulation results; 2) the experimental results respond slightly slower than that of the simulation results since the existence of time delay of the real-time controller.

Thereafter, the performance of the proposed control scheme and the related simulation results are validated in the experiment, with two cases in Section V-A and Section V-D as examples. The parameters used in the experiment are the same as the simulation analysis. Firstly, the dynamics of VSG during the transient process in case 2 with different control schemes under U_g=0.15 pu are observed based on the oscilloscope. As shown in Fig. 21(a)-(c), it could be found that the proposed control scheme makes better performance compared with the method in [12], which achieves all of the three control objectives of VSG. Secondly, the dynamics of VSG during the transient process in case 2 with or without fault information under U_g=0.3 pu are observed based on the oscilloscope. According to Fig. 22(a)-(c), the performance of the proposed control scheme without the fault information is very close to the method in [27] which requires the fault-detecting device.

Obviously, the experimental results in Fig. 21 and Fig. 22 align with the related simulation results in Fig. 13 and Fig. 19. Therefore, the effectiveness of the proposed control scheme and the simulation results are further validated by the OPAL-RT real-time simulation platform.

VII. Conclusions

A non-fault information based dual-loop adaptive feedback control is proposed in this paper, which can simultaneously achieve the three control objectives of transient angle stability, current limitation and the requirement of the grid code for the reactive current of VSG during fault such as a serious grid voltage sag. First, the large-signal models of VSG and the paralleled system of VSG and VSC are built respectively with a dual-loop feedback control. Subsequently, the feasible coefficient region of the feedback coefficients in APCL and RPCL under different fault degrees and cases are studied. The change rule provides reference for the curve fitting, which is further applied in the self-adaptive regulation of the feedback coefficients. Therefore, a dual-loop adaptive feedback control based on an additional reactive power feedback loop is proposed. With the proposed control scheme, all of the three control objectives can be achieved since the feedback coefficients are within the feasible coefficient region due to the self-adaptive regulation. Finally, the effectiveness and robustness of the proposed control scheme in both VSG and the paralleled system of VSG and VSC are validated with simulation results and experimental results.

References

[1] J. Rocabert, A. Luna, F. Blaabjerg, and P. Rodríguez, "Control of power converters in AC microgrids," *IEEE Trans. Power Electron.*, vol. 27, no. 11, pp. 4734-4749, Nov. 2012.

[2] Q. Zhong, P. Nguyen, Z. Ma, and W. Sheng, "Self-synchronized synchronverters: inverters without a dedicated synchronization unit," *IEEE Trans. Power Electron.*, vol. 29, no. 2, pp. 617-630, Feb. 2014.

[3] Z. Shuai, W. Huang, C. Shen, J. Ge, and J. Shen, "Characteristics and restraining method of fast transient inrush fault currents in synchronverters," *IEEE Trans. Ind. Electron.*, vol. 64, no. 9, pp. 7487-7497, Sep. 2017.

[4] H. Lin, C. Jia, J. M. Guerrero, and J. C. Vasquez, "Angle stability analysis for voltage-controlled converters," *IEEE Trans. Ind. Electron.*, vol. 64, no. 8, pp. 6265-6275, Aug. 2017.

[5] X. Wang, M. G. Taul, H. Wu, Y. Liao, F. Blaabjerg, and L. Harnefors, "Grid-synchronization stability of converter-based resources-an overview," *IEEE Open J. Ind. Appl.*, vol. 1, pp. 115-134, Aug. 2020.

[6] Z. Shuai, C. Shen, X. Liu, Z. Li, and Z. Shen, "Transient angle stability of virtual synchronous generators using Lyapunov's direct method," *IEEE Trans. Smart Grid*, vol. 10, no. 4, pp. 4648-4661, Jul. 2019.

[7] X. Xiong, C. Wu, B. Hu, D. Pan, and F. Blaabjerg, "Transient damping method for improving the synchronization stability of virtual synchronous generators," *IEEE Trans. Power Electron.*, vol. 36, no. 7, pp. 7820-7831, Jul. 2021.

[8] X. Xiong, C. Wu, P. Cheng, and F. Blaabjerg, "An optimal damping design of virtual synchronous generators for transient stability enhancement," *IEEE Trans. Power Electron.*, vol. 36, no. 10, pp. 11026-11030, Apr. 2021.

[9] D. Pan, X. Wang, F. Liu, and R. Shi, "Transient stability of voltage-source converters with grid-forming control: a design-oriented study," *IEEE J. Emerg. Sel. Topics Power Electron.*, vol. 8, no. 2, pp. 1019-1033, Jun. 2020.

[10] X. Xiong, C. Wu, D. Pan, and F. Blaabjerg, "An improved synchronization stability method of virtual synchronous generators based on frequency feedforward on reactive power control loop," *IEEE Trans. Power Electron.*, vol. 36, no. 8, pp. 9136-9148, Aug. 2021.

[11] P. Ge, C. Tu, F. Xiao, Q. Guo, and J. Gao, "Design-oriented analysis and transient stability enhancement control for a virtual synchronous generator," *IEEE Trans. Ind. Electron.*, vol. 70, no. 3, pp. 2675-2684, Mar. 2023.

[12] H. Wu and X. Wang, "A mode-adaptive power-angle control method for transient stability enhancement of virtual synchronous generators," *IEEE J. Emerg. Sel. Top. Power Electron.*, vol. 8, no. 2, pp. 1034-1049, Jun. 2020.

[13] M. Chen, D. Zhou, and F. Blaabjerg, "Enhanced transient angle stability control of grid-forming converter based on virtual synchronous generator," *IEEE Trans. Ind. Electron.*, vol. 69, no. 9, pp. 9133-9144, Sep. 2020.

[14] L. Huang, H. Xin, Z. Wang, L. Zhang, K. Wu, and J. Hu, "Transient stability analysis and control design of droop-controlled voltage source converters considering current limitation," *IEEE Trans. Smart Grid*, vol. 10, no. 1, pp. 578-591, Jan. 2019.

[15] E. Rokrok, T. Qoria, A. Bruyere, B. Francois, and Xavier Guillaud, "Transient stability assessment and enhancement of grid-forming converters embedding current reference saturation as current limiting strategy," *IEEE Trans. Power Syst.*, vol. 37, no. 2, pp. 1519-1531, Mar. 2022.

[16] L. Zhang, L. Harnefors, and H. P. Nee, "Power-synchronization control of grid-connected voltage-source converters," *IEEE Trans. Power Syst.*, vol. 25, no. 2, pp. 809-820, May 2010.

[17] A. D. Paquette and D. M. Divan, "Virtual impedance current limiting for inverters in microgrids with synchronous generators," *IEEE Trans. Ind. Appl.*, vol. 51, no. 2, pp. 1630-1638, Mar. 2015.

[18] M. G. Taul, X. Wang, P. Davari, and F. Blaabjerg, "Current limiting control with enhanced dynamics of grid-forming converters during fault conditions," *IEEE J. Emerg. Sel. Top. Power Electron.*, vol. 8, no. 2, pp. 1062-1073, Jun. 2019.

[19] T. Qoria, F. Gruson, F. Colas, G. Denis, T. Prevost, and X. Guillaud, "Critical clearing time determination and enhancement of grid-forming converters embedding virtual impedance as current limitation algorithm," *IEEE J. Emerg. Sel. Top. Power Electron.*, vol. 8, no. 2, pp. 1050-1061, Jun. 2020.

[20] T. Liu, X. Wang, F. Liu, K. Xin, and Y. Liu, "A current limiting method for single-loop voltage-magnitude controlled grid-forming converters during symmetrical faults," *IEEE Trans. Power Electron.*, vol. 37, no. 4, pp. 4751-4763, Apr. 2022.

[21] Z. Jin and X. Wang, "A dq-frame asymmetrical virtual impedance control for enhancing transient stability of grid-forming inverters," IEEE Trans. Power Electron., vol. 37, no. 4, pp. 4535-4544, Apr. 2022.

[22] E. O. N. Netz, "Grid code-high and extra high voltage," E. ON Netz GmbH, Bayreuth, Apr. 2006.

[23] H. Geng, L. Liu, and R. Li, "Synchronization and reactive current support of PMSG-based wind farm during severe grid fault," *IEEE Trans. Sustain. Energy*, vol. 9, no. 4, pp. 1596-1604, Oct. 2018.

[24] H. Wu and X. Wang, "Design-oriented transient stability analysis of PLL-synchronized voltage-source converters," *IEEE Trans. Power Electron.*, vol. 35, no. 4, pp. 3573-3589, Apr. 2020.

[25] K. Sun, W. Yao, J. Wen, and L. Jiang, "A two-stage simultaneous control scheme for the transient angle stability of VSG considering current limitation and voltage support," *IEEE Trans. Power Syst.*, vol. 37, no. 3, pp. 2137-2150, May. 2022.

[26] K. Sun, W. Yao, and J. Wen, "Dual-loop PQ control scheme for transient stability enhancement and current limitation of VSG," in *Proc. 13th Int. Conf. Power Syst. Tech.*, Haikou, China, 2021, pp. 1732-1736.

[27] P. Ge, F. Xiao, C. Tu, Q. Guo, J. Gao, and Y. Song, "Comprehensive transient stability enhancement control of a VSG considering power angle stability and fault current limitation," *CSEE J. Power Energy Syst.*, DOI: 10.17775/CSEEJPES.2021.00340, 2022, In Press.

[28] "IEEE Recommended Practice for Monitoring Electric Power Quality," IEEE Std. 1159-2019, pp. 1-98, Aug. 2019.

[39] "IEEE standard for interconnection and interoperability of distributed energy resources with associated electric power systems interfaces," IEEE Std. 1547-2018, pp. 1-72, Apr. 2018.

[30] J. Alipoor, Y. Miura, and T. Ise, "Stability assessment and optimization methods for microgrid with multiple VSG units," *IEEE Trans. Smart Grid*, vol. 9, no. 2, pp. 1462-1471, Mar. 2018.

[31] M. G. Taul, X. Wang, P. Davari, and F. Blaabjerg, "Reduced-order and aggregated modeling of large-signal synchronization stability for multi-converter systems," *IEEE J. Emerg. Sel. Top. Power Electron.*, vol. 9, no. 3, pp. 3150-3165, Jun. 2021.

[32] H. Cheng, Z. Shuai, C. Shen, X. Liu, Z. Li, and Z. Shen, "Transient angle stability of paralleled synchronous and virtual synchronous generators in islanded microgrids," *IEEE Trans. Power Electron.*, vol. 35, no. 8, pp. 8751-8765, Aug. 2020.

[33] X. He and H. Geng, "Transient stability of power systems integrated with inverter-based generation," *IEEE Trans. Power Syst.*, vol. 36, no. 1, pp. 553-556, Jan. 2021.

[34] H. Yuan, X. Yuan, and J. Hu, "Modeling of grid-connected VSCs for power system small-signal stability analysis in DC-link voltage control timescale," *IEEE Trans. Power Syst.*, vol. 32, no. 5, pp. 3981-3991, Sep. 2017.

[35] R. Liu, J. Yao, X. Wang, P. Sun, J. Pei, J. Hu, and F. Blaabjerg, "Dynamic stability analysis and improved LVRT schemes of DFIG-based wind turbines during a symmetrical fault in a weak grid," *IEEE Trans. Power Electron.*, vol. 35, no. 1, pp. 303-318, Jan. 2020.

Kun Sun received the B.S., M.Sc., and Ph.D. degrees in electrical engineering from Huazhong University of Science and Technology (HUST), Wuhan, China, in 2015, 2018, and 2022, respectively. From 2019 to 2020, he was a Visiting Ph.D. Student with the Department of Energy Technology, Aalborg University, Aalborg, Denmark. Currently, he has been a Senior Engineer with the Power Dispatching and Control Center, China Southern Power Grid Company, Ltd., Guangzhou, China. His current research interests include stability analysis and control of renewable energy integration.

Wei Yao (Senior Member, IEEE) received the B.S. and Ph.D. degrees in electrical engineering from Huazhong University of Science and Technology (HUST), Wuhan, China, in 2004 and 2010, respectively. He was a Post-Doctoral Researcher with the Department of Power Engineering, HUST, from 2010 to 2012 and a Postdoctoral Research Associate with the Department of Electrical Engineering and Electronics, University of Liverpool, Liverpool, U.K., from 2012 to 2014. Currently, he has been a Professor with the School of Electrical and Electronics Engineering, HUST, Wuhan, China. His current research interests include power system stability analysis and control, renewable energy, HVDC and DC Grid, and application of artificial intelligence in Smart Grid.

Qihang Zong received the B.S. degree in electrical engineering from Hefei University of Technology, Hefei, China, in 2021. He is currently working toward the Ph.D. degree in electrical engineering at Huazhong University of Science and Technology (HUST). His research interests include transient stability analysis and control of power system with renewable energy.

Jinyu Wen (Member, IEEE) received the B.S. and Ph.D. degrees in electrical engineering from Huazhong University of Science and Technology (HUST), Wuhan, China, in 1992 and 1998, respectively. He was a Visiting Student from 1996 to 1997 and Research Fellow from 2002 to 2003 all at the University of Liverpool, Liverpool, UK, and a Senior Visiting Researcher at the University of Texas at Arlington, Arlington, USA, in 2010. From 1998 to 2002 he was a Director Engineer with XJ Electric Co. Ltd. in China. In 2003, he joined the HUST and now is a Professor with the School of Electrical and Electronics Engineering, HUST. His current research interests include renewable energy integration, energy storage, multi-terminal HVDC and power system operation and control.

Lin Jiang (Member, IEEE) received the B.Sc. and M.Sc. degrees in electrical engineering from the Huazhong University of Science and Technology, Wuhan, China and the Ph.D. degree in electrical engineering from the University of Liverpool, Liverpool, U.K., in 1992, 1996, and 2001, respectively. He was a Postdoctoral Research Assistant with the University of Liverpool, Liverpool, U.K., from 2001 to 2003 and the Postdoctoral Research Associate with the Department of Automatic Control and Systems

Engineering, University of Sheffield, Sheffield, U.K., from 2003 to 2005. He was a Senior Lecturer with the University of Glamorgan, Pontypridd, U.K., from 2005 to 2007 and joined the University of Liverpool in 2007. He is currently a Reader with the Department of Electrical Engineering and Electronics, University of Liverpool. His research interests include control and analysis of power system, smart grid, and renewable energy.